Texturing of titanium (Ti6Al4V) medical implant surfaces with MHz-repetition-rate femtosecond and picosecond Yb-doped fiber lasers

Mutlu Erdoğan,[1,*] **Bülent Öktem,**[1] **Hamit Kalaycıoğlu,**[2] **Seydi Yavaş,**[1] **Pranab K. Mukhopadhyay,**[2] **Koray Eken,**[3] **Kıvanç Özgören,**[1] **Yaşar Aykaç,**[4] **Uygar H. Tazebay,**[5,6] **and F. Ömer Ilday**[2]

[1]*Materials Science and Nanotechnology Graduate Program, Bilkent University, Ankara 06800, Turkey*
[2]*Physics Department, Bilkent University, Ankara 06800, Turkey*
[3]*FiberLAST Ltd., Ankara 06531, Turkey*
[4]*Faculty of Dentistry, Ankara University, Ankara 06100, Turkey*
[5]*Molecular Biology and Genetics Department, Bilkent University, Ankara 06800, Turkey*
[6]*BILGEN, Bilkent University Genetics and Biotechnology Research Center, Ankara 06800, Turkey*

[*]*mutlu@bilkent.edu.tr*

Abstract: We propose and demonstrate the use of short pulsed fiber lasers in surface texturing using MHz-repetition-rate, microjoule- and sub-microjoule-energy pulses. Texturing of titanium-based (Ti6Al4V) dental implant surfaces is achieved using femtosecond, picosecond and (for comparison) nanosecond pulses with the aim of controlling attachment of human cells onto the surface. Femtosecond and picosecond pulses yield similar results in the creation of micron-scale textures with greatly reduced or no thermal heat effects, whereas nanosecond pulses result in strong thermal effects. Various surface textures are created with excellent uniformity and repeatability on a desired portion of the surface. The effects of the surface texturing on the attachment and proliferation of cells are characterized under cell culture conditions. Our data indicate that picosecond-pulsed laser modification can be utilized effectively in low-cost laser surface engineering of medical implants, where different areas on the surface can be made cell-attachment friendly or hostile through the use of different patterns.

© 2011 Optical Society of America

OCIS codes: (140.3390) Laser materials processing; (140.3510) Laser, fiber; (320.7090) Ultrafast lasers; (170.1850) Dentistry.

References and links

1. I. Etsion, "State of the art in laser surface texturing," J. Tribol. **127**, 248–253 (2005).
2. K. Anselme, "Osteoblast adhesion on biomaterials," Biomaterials **21**, 667–681 (2000).
3. R. Branemark, P-I Branemark, B. Rydevik, and R. R. Myers, "Osseointegration in skeletal reconstruction and rehabilitation: a review," J. Rehabil. Res. Dev. **38**(2), 175–181 (2000).
4. J. B. Park, *The Biomedical Engineering Handbook: Second Edition*, Joseph D. Bronzino, ed. (CRC Press LLC, 2000), Vol. II.

5. I. Degasne, M. F. Basle, V. Demais, G. Hure, M. Lesourd, B. Grolleau, L. Mercier, and D. Chappard, "Effects of roughness, fibronectin and vitronectin on attachment, spreading, and proliferation of human osteoblast-like cells (Saos-2) on titanium surfaces," Calcif. Tissue Int. **64**, 499–507 (1999).

6. L. Hao, J. Lawrence, Y. F. Phua, K. S. Chian, G. C. Lim, and H. Y. Zheng, "Enhanced human osteoblast cell adhesion and proliferation on 316 LS stainless steel by means of CO_2 laser surface treatment," J. Biomed. Mater. Res., Part B: Appl. Biomater. **73B**, 146–156 (2005).

7. A. C. Duncan, F. Weisbuch, F. Rouais, S. Lazare, and Ch. Baquey, "Laser microfabricated model surfaces for controlled cell growth," Biosens. Bioelectron. **17**, 413–426 (2002).

8. S. I. Anisimov and B. Rethfeld, "Theory of ultrashort laser pulse interaction with a metal," Proc. SPIE **3093**, 192–203 (1997).

9. C. Momma, S. Nolte, B. N. Chichkov, F. v. Alvensleben, and A. Tunnermann, "Precise laser ablation with ultra-short pulses," Appl. Surf. Sci. **109-110**, 15–19 (1997).

10. M. Trtica, B. Gakovic, D. Batani, T. Desai, P. Panjan, and B. Radak, "Surface modifications of a titanium implant by a picosecond Nd:YAG laser operating at 1064 and 532 nm," Appl. Surf. Sci. **253**, 2551–2556 (2006).

11. A. Y. Vorobyev and C. Guo, "Femtosecond laser nanostructuring of metals," Opt. Express **14**, 2164–2169 (2006).

12. A. Y. Vorobyev and C. Guo, "Femtosecond laser structuring of titanium implants," Appl. Surf. Sci. **253**, 7272–7280 (2007).

13. E. Fadeeva, S. Schlie, J. Koch, B. N. Chichkov, A. Y. Vorobyev, and C. Guo, "Femtosecond laser-induced surface structures and their effects on surface wettability and fibroblast cell proliferation," in *Contact Angle, Wettability and Adhesion* (Koninklijke Brill NV, 2009), pp. 163–171.

14. A. Y. Vorobyev and C. Guo, "Femtosecond laser surface structuring of biocompatible metals," Proc. SPIE **7203**, 720321 (2009).

15. A. Chong, J. Buckley, W. Renninger, and F. W. Wise, "All-normal-dispersion femtosecond fiber laser," Opt. Express **14**, 10095–10100 (2006).

16. F. Ö. Ilday, J. R. Buckley, W. G. Clark, and F. W. Wise, "Self-similar evolution of parabolic pulses in a laser," Phys. Rev. Lett. 92, 213902 (2004).

17. P. K. Mukhopadhyay, K. Özgören, I. L. Budunoglu, and F. Ö. Ilday, "All-fiber low-noise high-power femtosecond Yb-fiber amplifier system seeded by an all-normal dispersion fiber oscillator," IEEE J. Sel. Top. Quantum Electron. **15**, 145–152 (2009).

18. H. Kalaycioglu, B. Oktem, C. Senel, P. P. Paltani, and F. Ö. Ilday, "Micro joule-energy, 1 MHz-repetition rate pulses from an all-fiber-integrated nonlinear chirped-pulse amplifier," Opt. Lett. **35**, 959–961 (2010).

19. M. Jayaraman, U. Meyer, M. Bhner, U. Joos, and H. P. Wiesmann, "Influence of titanium surfaces on attachment of osteoblast-like cells in vitro," Biomaterials **25**(4), 625–631 (2004).

20. I. Degasne, M. F. Basl, V. Demais, G. Hur, M. Lesourd , B. Grolleau, L. Mercier, and D. Chappard "Effects of roughness, fibronectin and vitronectin on attachment, spreading, and proliferation of human osteoblast-like cells (Saos-2) on titanium surfaces," Calcif. Tissue Int. **64**(6), 499–507(1999).

21. U. Mayr-Wohlfart, J. Fiedler, K. P. Gnther, W. Puhl, and S. Kessler "Proliferation and differentiation rates of a human osteoblast-like cell line (SaOS-2) in contact with different bone substitute materials," J. Biomed. Mater. Res. **57**(1), 132–139.(2001).

22. Y. P. Kathuria, "Laser microprocessing of metallic stent for medical therapy," J. Mater. Process. Technol. **170**(3), 545–550 (2005).

23. K. Weman, *Welding Processes Handbook* (CRC Press LLC, 2003).

24. I. Etsion, "Improving tribological performance of mechanical components by laser surface texturing," Tribol. Lett. **17**, 733–737 (2004).

25. S. P. S. Porto, P. A. Fleury, and T. C. Damen, "Raman spectra of TiO2, MgF2, Zn F2, FeF2, and MnF2," Phys. Rev. **154**, 522–526 (1967).

26. H. L. Ma, J. Y. Yang, Y. Dai, Y. B. Zhang, B. Lu, and G. H. Ma, "Raman study of phase transformation of TiO2 rutile single crystal irradiated by infrared femtosecond laser," Appl. Surf. Sci. **253**, 7497–7500 (2007).

27. D. Buser, T. Nydegger, T. Oxland, D. L. Cochran, R. K. Schenk, H. P. Hirt, D. Snetivy, and L.-P. Nolte, "Interface shear strength of titanium implants with a sandblasted and acid-etched surface: a biomechanical study in the maxilla of miniature pigs," J. Biomed. Mater. Res. **45**(2), 75–83 (1999).

28. D. Y. Sullivan, R. L. Sherwood, and T. N. Mai, "Preliminary results of a multicenter study evaluating a chemically enhanced surface for machined commercially pure titanium implants," J. Prosthet. Dent. **78**(4), 379–386 (1997).

29. P. Uttayarat, G. K. Toworfe, F. Dietrich, P. I. Lelkes, and R. J. Composto, "Topographic guidance of endothelial cells on silicone surfaces with micro- to nanogrooves: orientation of actin filaments and focal adhesions," J. Biomed. Mater. Res. **75A**, 668–680 (2005).

30. J. A. Alaerts, V. M. De Cupere, S. Moser, P. van den Bosh de Aguilar, and P. G. Rouxhet, "Surface characterization of poly(methyl methacrylate) microgrooved for contact guidance of mammalian cells," Biomaterials **22**(12), 1635–1642 (2001).

1. Introduction

Surface engineering of materials using pulsed lasers is increasingly used to control and improve mechanical, chemical and even biological properties of surfaces since it is fast, environmentally friendly and offers excellent precision [1]. Surface chemistry, surface energy and topography play an essential role in cell adhesion on the surface, thus affecting the cell's ability to proliferate and differentiate [2]. This is particularly important for the effectiveness of medical implants to establish a mechanically stable integration of bone tissue and implant material surface [3]. Due to its good mechanical and chemical characteristics, including corrosion resistivity, relatively low density (4.5 g/cm^3), as well as biocompatibility, titanium is commonly used as implant material, particularly in dentistry, as bone plating, screws and hard tissue replacements. Both pure Ti and its certain alloys are used for surgical implant applications. Among these, the alloy Ti6Al4V is very common, due to its low cost, and superior tensile and yield strength compared to pure Ti [4].

Surface topology is known to play an important role in cell adhesion to surfaces of biomaterials, various kinds of implant surface texturing methods, including the use of lasers, are used to increase cell attachment and subsequent proliferation [5–7]. However, the techniques commonly used to create surface textures in commercial applications are mechanical (machining, sand-blasting) or chemical methods (such as acid etching, oxidation), all of which lack the spatial selectivity that laser-based texturing can offer. In addition, these techniques have potentially undesirable contamination and environmental effects. While surface texturing can be performed using nanosecond or longer-pulsed lasers, they result in undesirable thermal effects, limiting the level of precision.

Thermo-physical response of the material is a function of the pulse duration and shows significant changes going from the nanosecond regime to the femtosecond regime. Although this phenomenon is complex and the details depend on the material, an important factor is the characteristic time of electron-phonon coupling, which is typically in the order of tens of picoseconds for solids. This means that under the action of pulses shorter than this time scale, the absorbed pulse energy is stored in the electron subsystem, whereas the lattice remains at its considerably lower temperature. This results in greatly reduced thermal effects, leading to highly precise and localized processing with little effect to the surrounding region [8,9].

Excellent precision can be obtained with ultrashort-pulsed solid state lasers [10–14]. However, all previous results with ultrashort pulses were at kHz- or Hz-level repetition rates. In addition, these are complex and costly devices; consequently their use in surface texturing of biomaterials has been confined to laboratory experiments. Ultrafast fiber lasers operating at much higher repetition rates offer great potential for surface texturing at high speed with their attractive features such as low cost, robust operation, compact size, low intensity noise and diffraction-limited beam quality.

Here, we demonstrate the use of home-built picosecond and femtosecond pulsed fiber laser systems in texturing of dental implant surfaces. It was not clear *a priori* if the use of MHz-level repetition rates and relatively low pulse energies of few microjoules or less would result in diminished performance. We show that various surface textures with micrometer- and nanometer-sized features can be created at high speed with excellent precision and repeatability. The results are compared with those obtained with a commercial nanosecond fiber laser, for which heat effects are significant and result in relatively reduced precision. To the best of our knowledge, this is the first application of an ultrafast pulsed fiber laser to surface engineering. The impact of the surface textures on the attachment and growth of the cells is investigated, which indicate certain topologies are cell attachment- and growth-friendly and others are hostile. In addition, we observe tendency of attached cells to align along the direction of the structures.

2. Materials and Methods

2.1. *Surface Texturing with the Fiber Lasers*
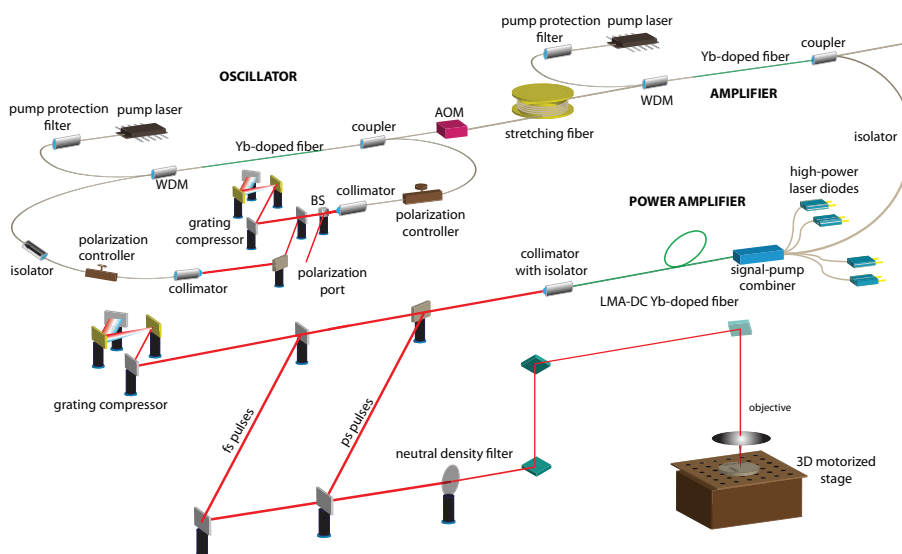
Fig. 1. Schematic diagram of the femtosecond all-fiber-integrated Yb amplifier and the material processing set-up, BS: beam splitter, AOM: acousto-optic modulator, LMA: large mode area, DC: double-clad.

The experimental setup is illustrated in Fig. 1. Two different, home-built fiber laser systems delivering picosecond and femtosecond pulses and a commercial nanosecond fiber laser (FL-NS-8W, FiberLAST) are used in these experiments. The nanosecond fiber laser produces 70 ns-long pulses at 20-200 kHz repetition rate and maximum average power of 8 W. One of the ultrafast laser systems is seeded by an all-normal-dispersion (ANDi) mode-locked Yb oscillator [15] with a central wavelength of 1060 nm and the other one by a self-similar mode-locked Yb oscillator [16] with a central wavelength of 1035 nm. The oscillator repetition rates are 43 MHz and 28 MHz, respectively. Both oscillators produce few picosecond-long, chirped pulses, which are fiber-coupled to all-fiber-integrated and misalignment-free amplifiers. First, the pulses are temporally stretched in fiber stretchers to reduce nonlinear effects, then traverse preamplifiers, which boost the power to 100-150 mW, which is sufficient to seed the power amplifiers. Both systems incorporate 10 ns-risetime fiber-coupled acousto-optic modulators (AOM) to optionally reduce the repetition rate to 1 MHz prior to amplification. The first system produces an average power of up to 16 W, corresponding to an estimated peak power of 20 kW for 20-ps pulses at 43 MHz of repetition rate. Following pulse compression with the gratings, pulse duration is measured to be 200 fs full-width at half-maximum (FWHM). The details of the system are described in [17]. The second system is used only at the reduced repetition rate of 1 MHz in order to maximize the pulse energy. The pulses are stretched to 150 ps in a 100-m long fiber stretcher and amplified to 104 nJ in the preamplifier. The nonlinear chirped-pulse power amplifier generates pulses with up to 4 μJ energy at 1 MHz repetition rate. The pulse duration is reduced to 80 ps during amplification as a result of gain filtering clipping the edges of the pulse in the time domain. The maximum peak power of amplified pulses is 57 kW and the compressed pulse duration is 150-200 fs. A detailed description of the second system is

provided in [18]. Both ultrafast systems can be used in picosecond mode by simply bypassing the pulse compressor. When the compressed pulses are used, they are always linearly polarized due to the grating compressor. Uncompressed pulses can be either unpolarized or optionally linearly polarized with a polarizer.

For processing with the home-built ultrafast fiber laser systems, the beam is focused to a spot diameter, adjustable in the range of 10-15 μm using a high-power and 1 μm-wavelength compatible microscopy objective. The processing setup comprises of a collimating telescope, the objective and a 3-axis motorized and computer-controlled translation stage. Various patterns can be formed on the surface by scanning the translation stage on which the samples are placed.

For processing with the commercial nanosecond pulsed fiber laser, the beam is scanned over the sample with a computer-controlled galvanometer-based scanner, using a special objective lens designed to maintain a uniform spot diameter irrespective of the deflection angle. The spot diameter in the focal plane is estimated to be approximately 40 μm. All three laser systems have nearly diffraction-limited beam quality ($M^2 < 1.2$) and they can be switched off within microseconds for jumping from one point to another. Scan rates used in the experiments range between 3 μm/s and 50 μm/s.

2.2. Cell Culture and Microscopy
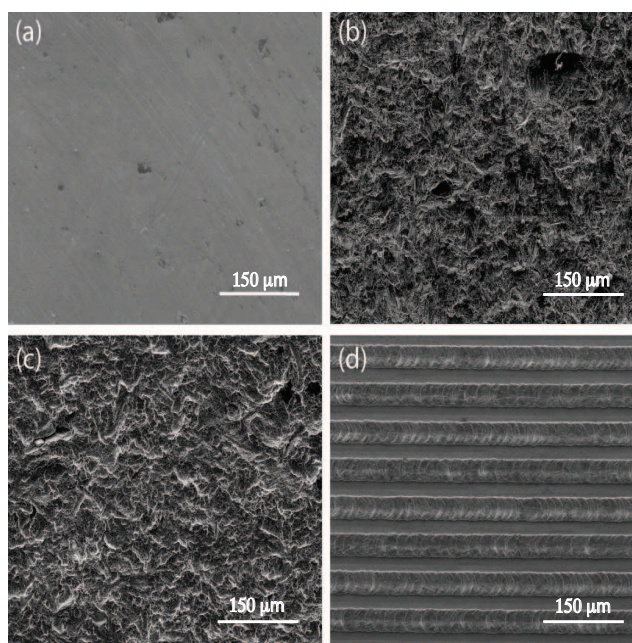
Fig. 2. Scanning electron microscope (SEM) images of three different commercial and one fiber laser-textured Ti disks that are subsequently used in cell attachment and proliferation assays. (a) Acid etched, (b) sand-blasted, (c) SLA and (d) fiber laser textured using the second laser system operating at 1 MHz with 1 W of average power, and 80 ps of pulse duration.

Human osteosarcoma cell line Saos-2 is widely used in studies on cell adhesion, proliferation and differentiation [19–21]. In this study, Saos-2 cells are cultured in McCoy's 5A medium supplemented with 15% fetal bovine serum, 2 mM L-glutamine, streptomycin/penicillin 100 U/mL, and in a humidified atmosphere of 95% air and 5% CO_2 at 37°C. Cells are seeded onto

8-mm diameter Ti (Ti6Al4V) disks with three different commercially modified surfaces and one fiber laser-modified surface, which are shown in Fig. 2.

Before use, all samples are sterilized for 30 minutes in 10% NaClO with an ultrasonic cleaner and placed in 24-well cell culture plates with a density of 100,000 cells/ml. Separate attachment tests are done for incubation periods of 36 hours and 7 days. At the end of the incubation periods, the disks are washed with PBS, treated with trypsin/EDTA solution for 20 seconds to eliminate the poorly attached cells, and then fixed in 0.1 M sodium cacodylate buffer with 3% glutaraldehyde, pH 7.2 at 4°C overnight. For each surface type, 3 Ti disks are used (samples are triplicated), hence 12 Ti disks are used for each incubation period in total. Following up the fixation stage, cells are stained with 300 nM 4, 6-diamidino-2-phenylindole, dilactate (DAPI, dilactate) in PBS and with Mitotracker Red 580 (Invitrogen) in McCoy's 5a and subsequently counted under a fluorescent microscope (Nikon Eclipse Ti/U).

3. Results and Discussion

We find that a large variety of surface patterns can be created using both the femtosecond and picosecond pulses by controlling the pulse energy, duration, exposure time and the scanning pattern (selected sample patterns are shown in Fig. 3 and Fig. 4).
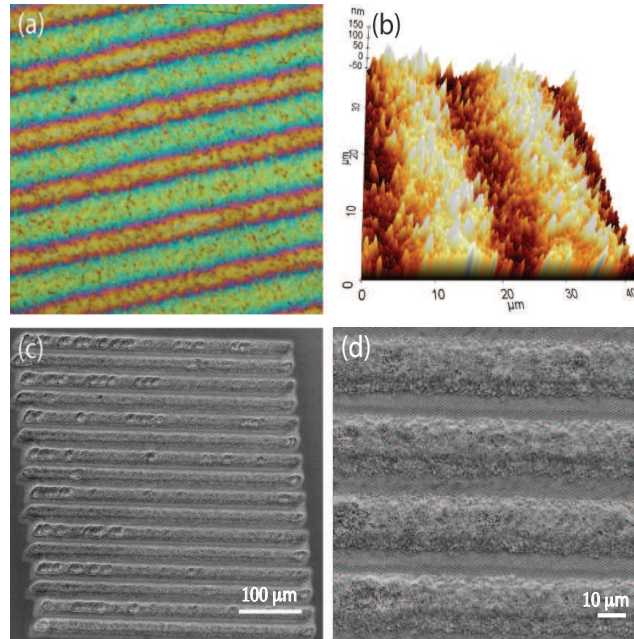
Fig. 3. Surface textures obtained using femtosecond pulses. Optical (a) and atomic force (b) microscope images of the nanometer-scale surface textures at low fluence. (c, d) SEM images of the micron-scale surface texturing created at high fluences.

For the creation of surface textures with micron-scale features, picosecond and femtosecond pulses yield similar results, as expected. Using femtosecond pulses at sufficiently low fluences (around 0.04 J/cm^2), it is possible to obtain nanoscale roughening of the surfaces. This appears not to be possible with picosecond pulses, which simply lead to creation of micron-scale structures with the scale set by the laser spot size on the surface. We attribute this difference to thermal effects occurring during the picosecond-long pulse, which wash away the fine nanometer-scale features, even though the thermal effects are greatly reduced compared to use

of nanosecond pulses.

Using femtosecond pulses, we produce nanoscale surface roughening at low fluences and micron-scale surface texturing at high fluences. Line patterns are formed on the Ti surface with incident power of 1.4 W, repetition rate of 43 MHz, pulse duration of 300 fs, scan rate of 4 μm/s, and spot diameter of 10 μm (Fig. 3(a) and (b)). The corresponding fluence is 0.04 J/cm^2. These conditions result in nanometer-scale modification of the surface with an average roughness of 100 nm. In contrast, a similar line pattern, however of micron-scale height, is formed when using incident power of 0.7 W, repetition rate of 1 MHz (corresponding to a pulse energy of 700 nJ), pulse duration of 400 fs, scan rate of 3 μm/s, and spot diameter of 10 μm (Fig. 3 (c) and (d)). The corresponding fluence is 0.89 J/cm^2. There is no heat-affected zone (HAZ), when using femtosecond pulses that can be discerned through scanning electron microscope (SEM) and atomic force microscope (AFM) images. Reducing HAZ is important since these heat affected zones are more susceptible to the formation of cracks that reduces the life-time of the metal implant [22, 23].
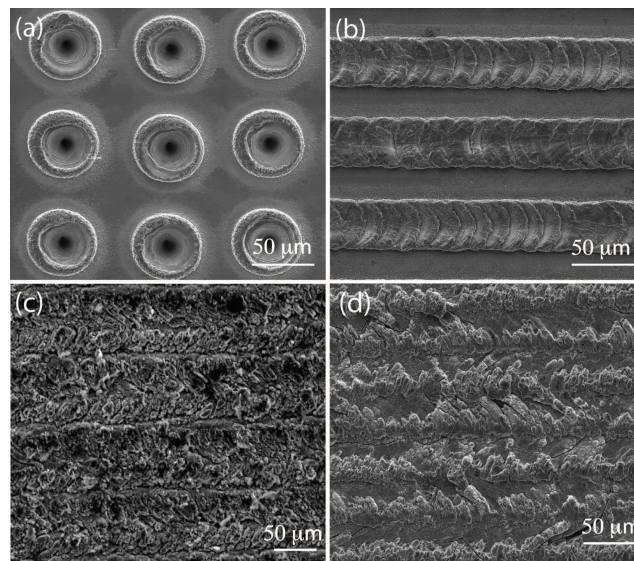
Fig. 4. SEM images of the micron-scale surface textures with dotted (a) and line-scan (b, c, d) structures formed with picosecond pulses.

Using picosecond pulses, microstructures with feature sizes of 10-20 μm and height contrast of approximately 5-10 μm are easily created. Fig. 4(a) shows SEM image of dot-pattern formed on the Ti surface using incident power of 2 W, repetition rate of 43 MHz, pulse duration of 20 ps, and approximately 40 μm of spot diameter. The corresponding fluence is 0.0037 J/cm^2. A line pattern is shown in Fig. 4(b), produced using incident power of 1 W, repetition rate of 1 MHz, pulse duration of 80 ps, scan rate of 3 μm/sec, and 10 μm of spot diameter. The corresponding fluence is 1.27 J/cm^2. Another pattern is shown in Fig. 4(c), created using incident power of 2 W, 43 MHz repetition rate, pulse duration of 25 ps, spot diameter of 10 μm, scan rate of 50 μm/sec and fluence of 0.0059 J/cm^2. The pattern is formed by line scans, with the parallel scan lines barely touching each other from the edges. The line pattern in Fig. 4(d) is produced using the same parameters as in Fig 4(c), but the parallel lines are overlapped by several micrometers from the edges. In the picosecond regime, a small HAZ is discernible around the microstructures, visible as contrast changes in the SEM image and with an extent of 10-15 μm. The surface patterns are mechanically stable and strong. The modified Ti surfaces were

repetitively subjected to 10% NaClO in an ultrasonic cleaner and proteolytic trypsin enzyme during cell attachment experiments. In addition, after nearly a year, during which a number of experiments have been performed, the laser-textured surfaces appear to be unchanged according to recent SEM images.

For comparison, we use the nanosecond fiber laser to produce surface textures. A dot-pattern (Fig. 5(a)) is produced using incident power of 1 W, pulse duration of 71 ns, repetition of 25 kHz, scan rate of 5 mm/sec, and spot diameter of approximately 40 μm. The corresponding fluence is 3.2 J/cm^2. SEM image of a line pattern formed with identical laser parameters are shown in Fig. 5(b). The nanosecond pulsed laser results in clearly more pronounced HAZ, extending up to approximately 50 μm, as well as a relatively reduced precision and repeatability.
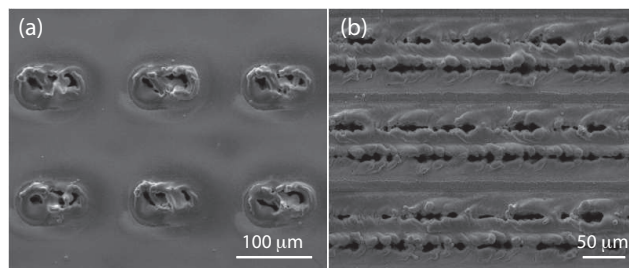
Fig. 5. SEM images of the micron-scale surface textures with dotted (a) and line (b) structures formed with nanosecond pulses.

For most surface texturing applications, including the creation of microdimples, the micron-scale control afforded by the picosecond fiber laser appears to be sufficient [24]. In order to better understand the process underlying of the texture formation, we employ energy-dispersive X-ray spectroscopy (EDX) analysis and Raman spectroscopy of the processed samples (Fig. 6).
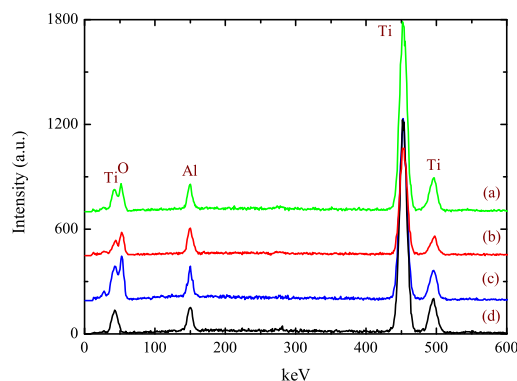
Fig. 6. EDX analysis of the Ti samples: the irradiated regions are (a) femtosecond, (b) picosecond, (c) nanosecond, and (d) unexposed region. The data lines are vertically displaced for clarity.

It is possible to produce micron-scale structures, which are either protrusions above or depressions on the surface. The height varies in the range of few micrometers, depending on the laser parameters. The EDX results indicate that oxygen is present in the processed regions, while it is absent in the unexposed areas. The concentration of oxygen in surface structures

appears to vary in the range of 25% to 35% for all pulse durations. This is consistent with the formation of TiO_2 as a result of the laser processing. Fig. 7 shows the Raman spectra covering 150-750 cm^{-1} of the processed Ti samples. As control, the non-irradiated area of the Ti samples does not present Raman activity. The irradiated areas result in three clear peaks located at 241, 439 and 613 cm^{-1}, which can be associated with the multi-photon process, E_g, and A_{1g} active Raman modes for the tetragonal rutile structure of TiO_2, respectively [25, 26]. Therefore, we conclude that the protruding structures formed by laser irradiation are largely composed of TiO_2 in the rutile phase, irrespective of the use of femtosecond, picosecond or nanosecond pulses.
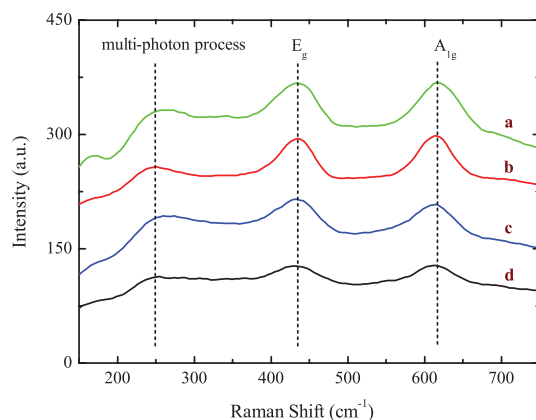
Fig. 7. Raman spectra of Ti samples: the irradiated regions by (a) femtosecond, (b) picosecond, (c) nanosecond pulses from the fiber lasers, and (d) unexposed region.

The effect of the surface textures created with the fiber laser on cell attachment and proliferation is evaluated through cell-culture experiments. We compare the picosecond laser-textured surfaces with three different commercially obtained implant surface types textured using sandblasting, acid etching and the SLA method. Following the methodology described above, we culture cells on indicated surfaces both for 36 hours (Fig. 8, left panel) to assess surface attachment, and for 7 days to monitor cell adhesion and proliferation (Fig. 8, right panel).
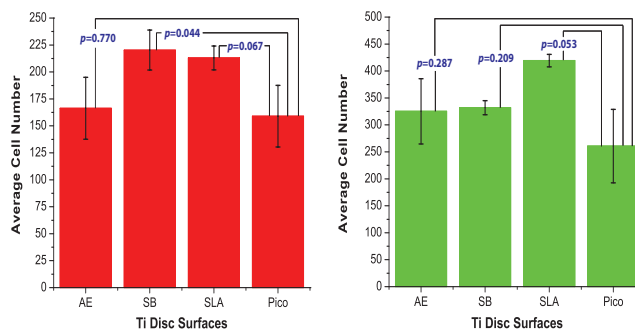
Fig. 8. Cell counts for analyzing attachment and proliferation after 36 hours (left) and 7 days (right). p values indicate the significance of experimental values obtained from commercial surfaces and picosecond laser treated surfaces according to two tailed t-test. AE: surfaces prepared using acid-etching; SB: surfaces prepared using sandblasting; SLA: surfaces prepared using the SLA method; Pico: surfaces prepared using the picosecond laser.

Both cellular attachment and proliferation on picosecond-laser-textured surface are as good as commercially used surfaces which are widely accepted to be surface textures of choice for stronger tissue integration [27, 28]. Binary comparisons of cellular tests on laser-textured surface with other modified surfaces (AE, SB, or SLA) indicated no significant difference in terms of attachment or proliferation according to a two-tailed t-test (Fig. 8) which is followed by statistical Bonferroni correction. (A p value of <0.02 was considered statistically significant).

We conclude that based on the cell attachment and cellular proliferation performance, the picosecond laser-textured surfaces are comparable to the commercially treated samples, within statistical fluctuations. Interestingly, as shown in Fig. 9, the cells tend to align with linear micron-size features formed by the picosecond laser-textured surfaces, a phenomenon known as topographical or contact guidance [29, 30]. However, there is no noticeable alignment on the surfaces with nanometer-scale height differences obtained with femtosecond pulses. Attachment is not improved either; we attribute this to the inadequate interaction between the cells and the nanoscale surface patterns (data not shown).

It appears possible to de-promote cell attachment and proliferation: with the dotted Ti surface pattern which is shown in Fig. 4 (a), the cells cultured on this surface result in significantly reduced attachment and proliferation. We attribute this to the biomechanics of the process: These holes have diameters around 40 μm and depth of approximately 15 μm; cells which fall inside a hole cannot attach properly and cannot proliferate. Possibly, they undergo a stress dependent programmed cell death process known as apoptosis, as assessed by aberrant nuclear stainings.
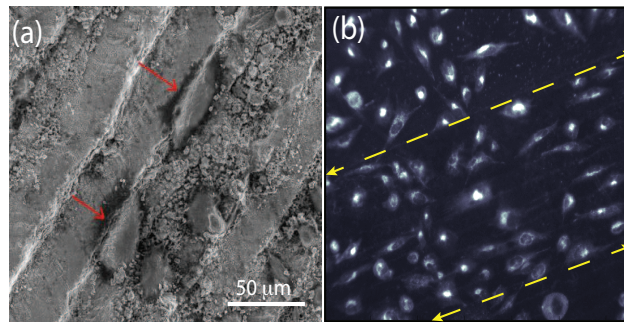
Fig. 9. (a) SEM image of osteosarcoma cells attached to a fiber laser textured Ti surface. The two red arrows indicate the cells aligned with linear features. (b) Fluorescent image of the same sample, where the cells are stained with DAPI and Mitotracker Red 580. The laser-textured area between the dashed (yellow) lines shows a general tendency of the cell population to align along the direction of the arrowheads.

4. Conclusion

In conclusion, we have demonstrated controlled surface texturing of Ti biomedical implant surfaces with high precision and repeatability using low-cost fiber lasers delivering picosecond and femtosecond pulses at 1 MHz and 43 MHz repetition rate. To the best of our knowledge, this is the first use of a pulsed fiber laser for surface texturing. In addition, we utilize repetition rates nearly 1000 times higher than in previous studies of ultrafast surface texturing. Given that the average power of the fiber amplifiers and the scanning speed can readily be scaled up, the use of MHz repetition rates holds great potential for significant improvements in processing speed, consequently, in the feasibility of ultrafast surface texturing for industrial applications. Comparison of the surface textures produced by the nanosecond-, picosecond- and

femtosecond-pulsed lasers validate the expected trend of diminishing heat effects as the pulse duration is decreased, thus improving precision and repeatability. However, we find that tens of picoseconds-long pulses are sufficient to reliably create micron-scale structures for control of cell attachment and proliferation. Given that picosecond operation of the laser does not require a grating compressor, and the laser beam is directly delivered from the optical fiber through a fiber collimator or a fiber focuser, the use of picoseconds pulses at MHz repetition rates holds remarkable potential for *in vivo* biomedical applications. Cell attachment and cell proliferation experiments indicate that laser-produced textures yield performance comparable within statistical deviations to commercially prepared surfaces using non-laser-based techniques. We find that different surface patterns can enhance or inhibit cell attachment; additional studies are needed for a full understanding of the effect of different patterns. A significant advantage of laser texturing is the capability to selectively treat different parts of an implant surface with different textures, which may be designed to enhance or inhibit cell attachment. Such spatial selectivity is not possible with conventional mechanical and chemical techniques.

While our emphasis has been on texturing of Ti-based implant surfaces, these results can easily be adapted to different materials and applications. We believe that ultrashort pulsed fiber laser technology is well-suited for widespread use in laser surface engineering and related applications outside of the research laboratory.

Acknowledgement